Title
The Development of Porous Graphite Material for Lithium-Ion Battery

Author
Lam, Yook

Publication Date
2021

Peer reviewed|Thesis/dissertation

UNIVERSITY OF CALIFORNIA

Los Angeles

The Development of Porous Graphite Material for Lithium-Ion Battery

A thesis submitted in partial satisfaction

of the requirements for the degree Master of Science

in Chemical Engineering

by

Yook Teng Lam

2021

ABSTRACT OF THE THESIS

The Development of Porous Graphite Material

for Lithium-Ion Battery

by

Yook Teng Lam

Master of Science in Chemical Engineering

University of California, Los Angeles, 2021

Professor Yunfeng Lu, Chair

Rechargeable lithium-ion battery is the foremost candidate for next generation large scale energy storage systems and hybrid electric vehicles. However, these applications require high power batteries that can operate under high current conditions. While graphite is the primary commercialized anode, it is believed that graphite hinders the high-rate performance of lithium-ion battery. Graphite has poor rate performance, relatively low initial coulombic efficiency, and potential safety issues due to its low de-/lithiation potential that can cause metallic lithium plating. In order to enhance the rate performance and reduce the first cycle irreversible capacity, the development of a porous graphite material was evaluated.

The thesis of Yook Teng Lam is approved.

Yuzhang Li

Carlos Morales-Guio

Yunfeng Lu, Committee Chair

University of California, Los Angeles

2021

TO MY FAMILY AND FRIENDS

Table of Contents

List of Figures

List of Tables

Acknowledgements

I would like to express gratitude to Dr. Lu for his guidance and show my appreciation towards members of the Lu Lab for their assistance, especially Jinhui Xu and Qingyang Yin.

I would also like to thank Dr. Yuzhang Li and Dr. Carlos Morales-Guio for being on my committee and reviewing this work.

Lastly, I am grateful for the love and support that my family, partner, and friends have given me.

1 Introduction

The emissions of greenhouse gases from the burning of fossil are the major causes of global warming and climate change. Renewable energy sources such as solar, wind, and water energy have been developed to combat the reliance on fossil fuels. However, these sources of energy are not always readily available due to the dependence on natural occurrences. A suitable, alternative candidate to act as a power source is a rechargeable battery such as lithium-ion battery (LIB). Lithium-ion battery is considered the best for next generation large-scale energy storage systems or electric vehicles (EVs) to overtake non-renewable energy sources.[28]

Lithium-ion battery offers high energy density, high power density, long cycle life, and it is inexpensive. While LIB is commonly used in portable electronics and transportation right now, its application is continuing to grow. Current commercial lithium-ion battery is largely made from a graphite anode and a diverse cathode family that includes $LiCoO_2$ (LCO), $LiFePO_4$ (LFP), $LiMn_2O_4$ (LMO), $LiNiO_2$ (LNO), $LiNi_{1-y-z}Co_yMn_zO_2$ (NMC), and $LiNi_{1-y-z}Co_yAl_zO_2$ (NCA).[23] Many different cathode materials have made their way to the market since the inception of LIB, but graphite continues to be the dominant anode and dominates 98 % of the market share while $Li_4Ti_5O_{12}$ (LTO) anode makes up the remaining 2 %.[1,3] This is attributed to graphite's relatively low cost, abundance, good conductivity, long cycle life, low de-/lithiation potential and high energy density.[4] However, the current electrochemical performance of graphite falters in meeting the increasing demand of advanced LIB for EVs and large-scale energy storage systems because graphite prevents high-rate performance of commercial LIB. Graphite has a much lower theoretical capacity of 372 mAh/g compared to alternative anodes such as silicon (4200 mAh/g), tin (993 mAh/g), and their alloys, hydrides, oxides, and phosphides.[17,20,31] However, these higher capacity candidates exhibit large volume expansion during lithium-ion insertion/extraction process which

leads to capacity loss over cycling. One of the ways to improving the performance of these materials is to use a buffer matrix such as carbon (e.g., graphite). The buffer matrix acts to mediate the expansion and preserve essential contact for charge transmission. On the contrary, the volume change is compensated to a limited degree therefore only offering moderate improvement in cycling stability. This issue needs to be addressed before these materials can be implemented.

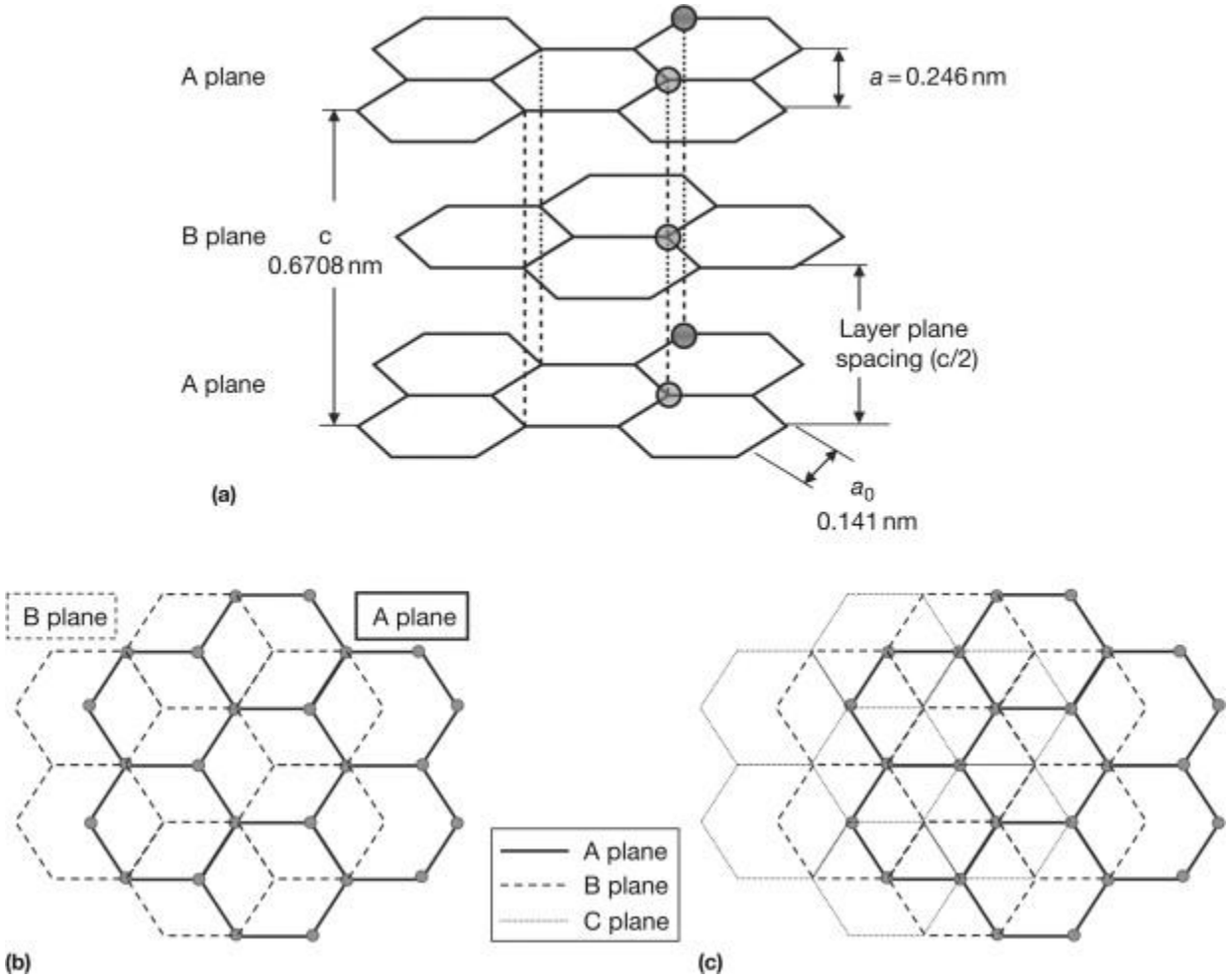

Figure 1. **(a)** Ideal crystal structure of graphite showing ABABAB sequence. **(b)** Top view of hexagonal graphite. **(c)** Top view of rhombohedral graphite.[39]

Graphite is the most successful anode material in LIB. It is constructed by a series of parallel sp^2 hybridized graphene layers, and in each layer, the carbon atom is covalently bonded to three other carbons forming a honeycomb lattice with a bond length of 0.142 nm. The fourth hybridized electron is free to migrate in the layer and it interacts with another delocalized electron in an adjacent layer by weak van der Waals forces. The distance between the layer planes is 0.335 nm. There are two forms of graphite which are distinguished by how the layers are stacked. Alpha or hexagonal graphite is stacked in ABABAB sequence with hexagonal symmetry in Figure 1b. Beta or rhombohedral graphite has ABCABCABC stacking order and the carbon atoms in every third layer are superimposed in Figure 1c. Rhombohedral graphite is less stable thermodynamically than hexagonal graphite and is rarely found in its pure form. Due to the layered structure, graphite has flake-like morphology with two different surfaces distinguished as the basal plane and edge plane in Figure 2. The edge plane is more reactive since it has greater surface area energy. Furthermore, the layered structure accounts for the anisotropic characteristic and affects the electronic, mechanical, and physiochemical properties of graphite. For example, the delocalized electrons allow electrical conduction within the basal plane but conduction across the edge plane is lower by three orders of magnitude. On the other hand, the weak van der Waals interactions of the layers enable intercalation of ions in between the planes forming graphite intercalation compounds (GICs). This leads to expansion of interlayer spacing and restacking of the graphene layers.

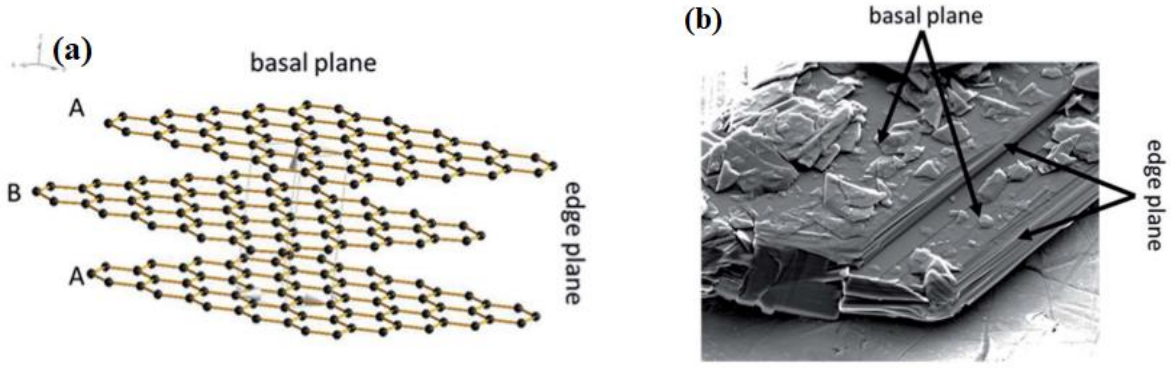

Figure 2. (a) Schematic illustration of the layered structure with basal plane and edge plane. **(b)** SEM of graphite particle showing basal plane and edge plane.[4]

Intercalation of secondary species into the planes of the graphite host is possible, and this is described by the staging phenomenon that was introduced by RÜdorff and Hofmann in 1938 in Figure 3.[14] The compounds are characterized by the 'nth stage compound' referring to the number of graphene layers between two intercalant layers. For example, a stage 4 compound has four graphene planes between the intercalants. As the concentration of intercalants increases inside the graphite, the number of empty layers decreases. The staging process is affected by the energy needed to expand spacing between two graphene planes and the repulsion between intercalant layers. However, the RÜdorff and Hofmann model cannot explain the transition from one stage to another assuming the graphene layers span the entire graphite crystal as mentioned by the researchers themselves. Daumas and Herold proposed a modified version to the RÜdorff and Hofmann model.[8] Stage 'n' compounds greater than stage 1 have flexible graphene layers and deform around domains or islands of the intercalated species. The islands are small relative to the size of the graphite crystal and stacked according to the RÜdorff and Hofmann model, therefore the ordering is maintained in a less rigid manner. In the transition of stages, for example from stage 3 to stage 2, the intercalants only need to diffuse within the same layer forming the next lower or

higher stage via intercalation or deintercalation. While studies have been conducted to provide evidence in support of the Daumas-Herold model, the staging mechanism remains to more complex than initially proposed and still requires further elucidation.

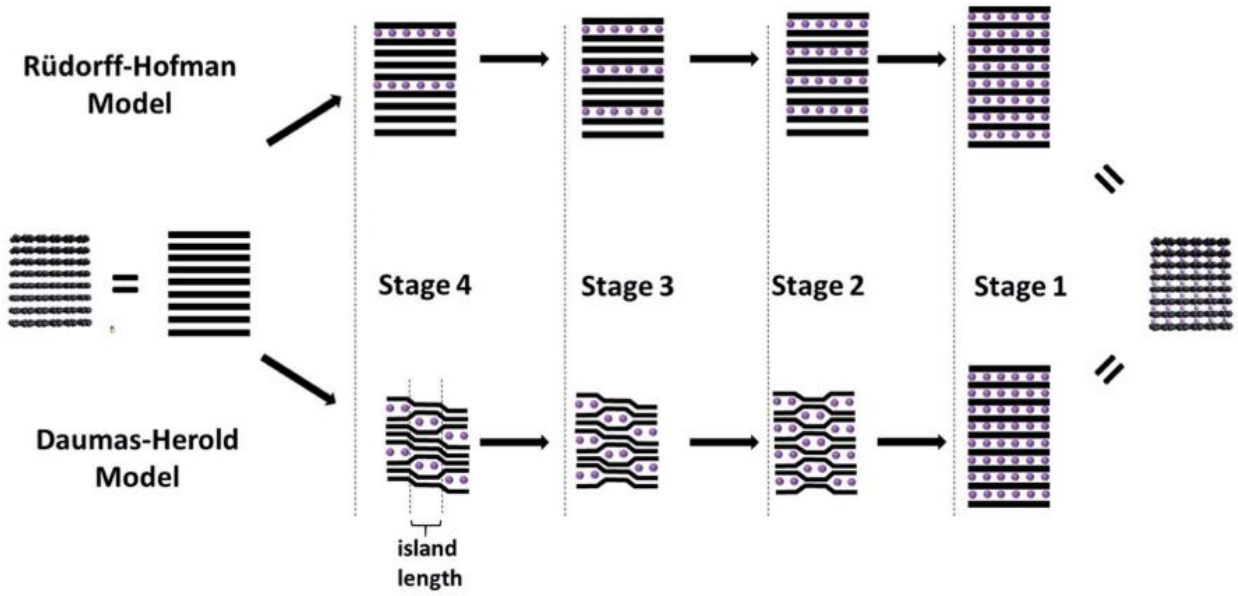

Figure 3. Schematic illustration of the intercalation mechanism into graphite host represented by the Rudorff Hoffman and Daumas-Herold Model.[4]

Graphite has garnered commercial success as the active material for the negative electrode because its layered structure allows for the insertion and extraction of lithium-ions within the interlayers, and the formation of lithium-graphite intercalation compound. The intercalation process is a reversible reaction during which lithium-carbon alloys (Li_xC_n) are formed.

$$C_n + xLi^+ + xe^- \leftrightarrow Li_xC_n$$

In the charging process, lithium-ions are loaded into graphite in several stages via the Daumas-Herold model in Figure 4. A highly crystalline graphite can form stage 1 lithium-graphite intercalation compound with phase LiC_6 which is the maximum possible lithium-ions that can be

inserted, and this accounts for its gravimetric capacity of 372 mAh/g. Since the discovery of this reversible intercalation behavior of lithium-ions into graphite, lithium intercalated graphite replaced lithium metal as anode in LIBs. Another reason for its success has to do with its advantage of having the lowest average de-/lithiation potential (i.e. 0.2 V vs Li/Li^+). This results in a voltage hysteresis between the charge and discharge potential to be relatively small and a greater energy efficiency. However, some intrinsic challenges remain with graphite anodes.

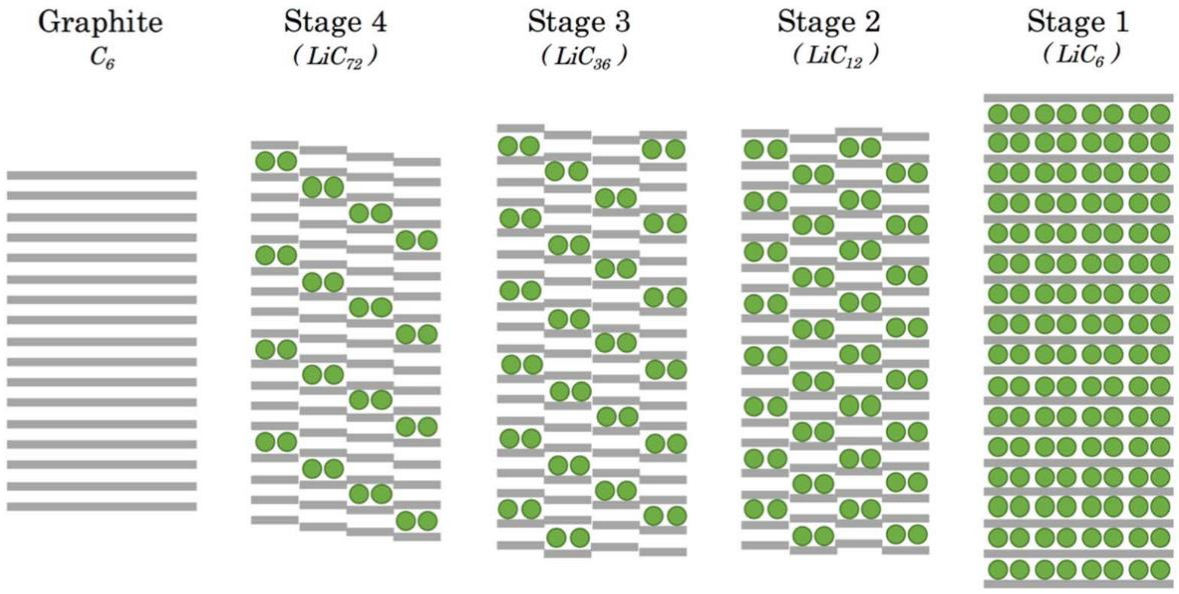

Figure 4. Schematic illustration of the staging mechanism and intercalation of lithium-ions into graphite host with the Daumas-Herold model.[2]

One of the major challenges is the limited rate capability of graphite especially for the lithiation process. Some studies have shown that lithium-ion diffusion between the graphene planes should be extremely fast in theory. KÜhne *et al*. investigated the lithium-ion diffusion process in bilayer graphene by performing time-dependent Hall voltage measurements and

determined a diffusion coefficient as high as 7 x 10^{-5} cm^2/s.[22] Persson *et al.* measured the diffusion of lithium-ions in highly oriented pyrolytic graphite (HOPG), which revealed that lithium-ion diffusivity in the direction parallel to the graphene plane is about 10^{-7} to 10^{-6} cm^2/s and in the perpendicular direction is about 10^{-11} cm^2/s (Figure 5. Diffusion of stage 2 (blue squares) and stage 1 (red circles) phases in the lithium-graphite system, which was obtained from kinetic Monte Carlo simulations based on first principles calculations.[21] The inset shows the path of lithium (blue circles) on the graphite lattice that was used to calculate lithium migration barriers.[35] However, experimental observations of standard electrodes have shown that the lithiation process is limited to a charge rate of 1C while the de-lithiation process can occur at a discharge rate as high as 10C. Persson *et al.* also determined the diffusivity to be about 10^{-7} cm^2/s for stage 1 and stage 2 HOPG with many vacancies but the value decreased to about 5 x 10^{-9} cm^2/s for both stages upon full lithiation.[35] Other factors that affect rate capability of graphite include the particle size and morphology, electrode design, phase transitions that occur, composition of the SEI, and the ambient temperature.

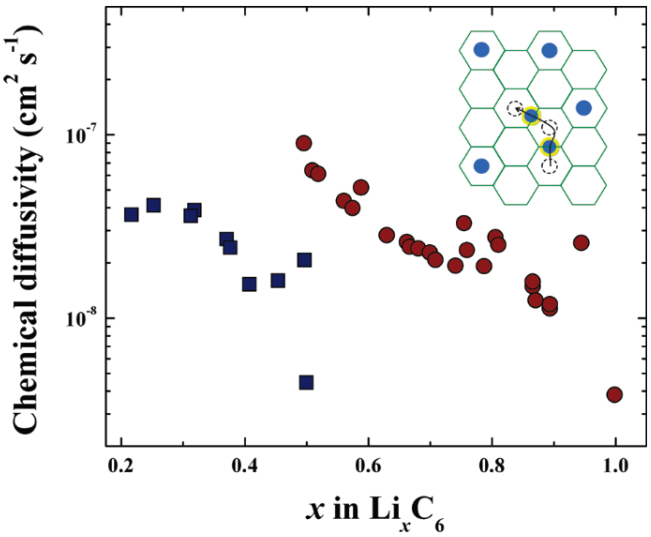

Figure 5. Diffusion of stage 2 (blue squares) and stage 1 (red circles) phases in the lithium-graphite system, which was obtained from kinetic Monte Carlo simulations based on first principles

calculations.[21] The inset shows the path of lithium (blue circles) on the graphite lattice that was used to calculate lithium migration barriers.[35]

Another drawback of graphite anodes in LIB is the first cycle irreversible capacity caused by the electrolyte decomposition and the consumption of lithium-ions as the charge carrier. One approach to reduce the first cycle irreversible capacity is to modify the graphite surface, such as chemically altering the basal and edge planes to improve the electrochemical performance. For example, Ein-Eli and Koch dispersed graphite in nitric acid or in a solution of $(NH_4)_2S_2O_4$ in sulfuric acid, then treated it with hot LiOH solution.[10] In both experiments, the SEI layer formed on the graphite surface reduced the extent of electrolyte decomposition which improved the initial coulombic efficiency and the reversible capacity. Other surface alteration studies are categorized by inorganic, organic polymer, and carbonaceous coatings. Incorporating metal composites or the metal coating generally facilitates the SEI formation and results in higher reaction kinetics for the de-/lithiation process due to increased charge transfer and less SEI resistance.[5,32,33] The use of metal fluorides and oxides coating may improve cycling stability, capacity retention, and/or higher initial coulombic efficiency.[9,11,18] Carbon coating is the most cost-efficient and may improve initial coulombic efficiency, but it can also significantly reduce the overall capacity in full cells. Furthermore, carbonaceous coatings may negatively affect the irreversible electrolyte decomposition should it cause an increased surface area of the active material.[40] The choice for carbon coatings should be selective, such as considering the particle morphology and composition. Another approach is to infuse electrolyte additives that kinetically favor the formation of the SEI layer so to enhance the initial coulombic efficiency. Fluoroethylene carbonate (FEC) improves the cycling efficiency and vinylene carbonate (VC) has been reported to stabilize the electrode/electrolyte interface by forming a polymeric film on the graphite surface before the

decomposition of ethylene carbonate (EC). Studies have also shown that VC as an additive in propylene carbonate (PC) solvent prevents (PC) co-intercalation and graphite exfoliation.[6] But VC reduces the cycling efficiency at high temperatures.[30] Vinyl ethylene carbonate (VEC) is more stable than VC and when VEC reductively decomposed on the graphite surface, there was improved performance and it prevented propylene carbonate (PC) co-intercalation into the anode.[16] Other additives such as ethylene sulfite and propylene sulfite have also been reported to suppress electrolyte decomposition, but their relatively low stability limits their utilization.[50]

Although ageing and resulting safety concerns are issues for all battery materials, they are especially important for graphite. The low de-/lithiation potential of graphite is close to the plating of metallic lithium, which may lead to potential plating of metallic lithium on the graphite surface. The ageing processes differ between the negative and positive electrode and are very complicated, requiring comprehensive analysis. The effects that the positive electrode have on the negative electrode must be considered as well. One investigated case is the diffusion and deposition of transition metal cations from the cathode to the anode. For example, Jahn-Teller distortions in spinel structures $LiMn_2O_4$ and $LiNi_{0.5}Mn_{1.5}O_4$ cause manganese dissolution and results in the formation of soluble Mn^{2+}.[7] This leads to capacity and power loss at the cathode and influences the SEI composition at the anode.[47] Another ageing process induced by the cathode is the decomposition of the electrolyte at high potentials and temperatures at the cathode surface. The decomposed electrolyte migrates to the anode leading to other side reactions or "cross-talking." [38] Sahore *et al.* constructed a two-compartment lithium-ion cell with a solid-state lithium-ion conductor as the separator to block the movement of species generated from one electrode to another. The cell was held long term at high voltage. They proposed that the cross-talk species were likely carbon-carbon double bonds and fluorinated carbons.[38] In respect to focusing only on

graphite, the ageing processes can be classified into three general categories: instability of the SEI long-term, lithium plating, and the effects of electrochemically inactive components such as the binder, conductive additives, and current collector. While the SEI layer is formed during the first cycle, its morphology and composition continuously evolve over cycling. Temperature influences the SEI layer through loss of lithium, electrolyte consumption, and an increase in resistance. These changes also affect the overall safety of the battery. Another safety issue is the potential plating of metallic lithium which can be caused by any increased overpotential for the lithiation process due to low operational temperature or elevated currents in Figure 6.

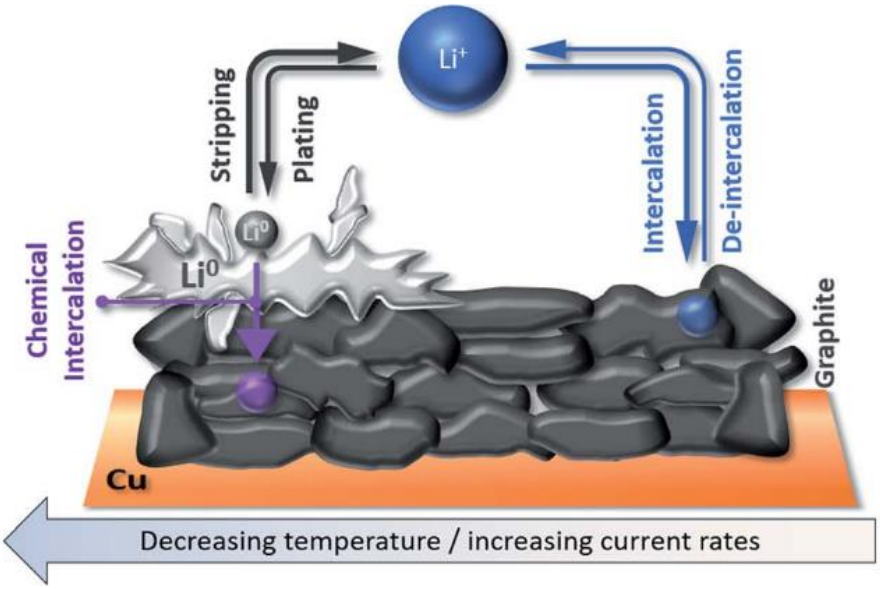

Figure 6. Schematic illustration of lithium plating and stripping on graphite electrode in competition with de-/intercalation of lithium ions into graphite depending on the applied current and temperature.[4,42]

Waldmann *et al.* studied the effects of temperature in the range –20 to 70 C had on lithium-ion cells and found that the rate of plating increases at lower temperatures due to slower lithium-ion diffusion.[43] LÜders *et al.* demonstrated that the extent of lithium plating is affected by the applied

current therefore limiting rapid charging of lithium-ion cell.[29] However, the rate of lithium plating decreases with cycling due to capacity fading over long-term cycling. The plated lithium metal reacts with the electrolyte and forms a layer on top of the graphite anode at high charging potentials at which the lithium metal is partially consumed. During the cycling process, some metallic lithium is re-oxidized and returned to the cathode while electronically insulated lithium continues to react with the electrolyte which leads to the formation of "dead" lithium species (Figure 7). In a study done by Fleischhammer *et al.*, the differences in safety behavior between un-aged and aged high-power lithium-ion cells were investigated by accelerating rate calorimetry and simultaneous thermal analysis. Cells that were aged by high rate and low temperature cycling exhibited lithium plating on the anode while those aged under high current conditions did not show significant differences.[12] These studies show that temperature plays a large role for ensuring long-term stable electrochemical performance.

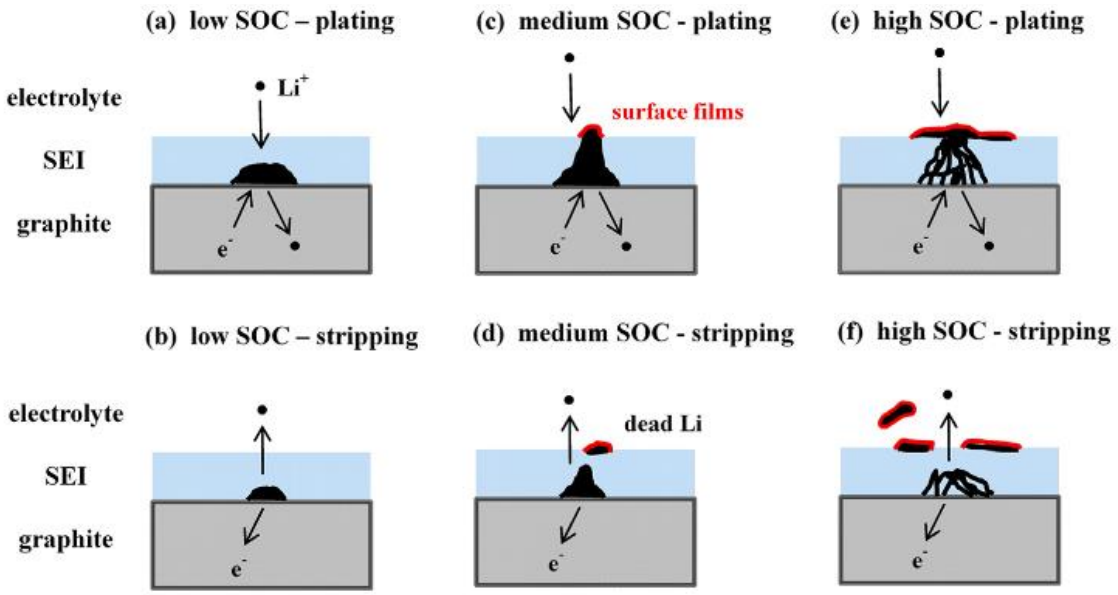

Figure 7. The lithium plating process on top of a graphite electrode at different SOC levels.[36]

Graphite intercalation compounds are formed by the insertion of chemical species or intercalants between the layers of the graphite host. These are compounds of particular interest due to their high degree of structural ordering relative to other intercalation compounds. Intercalation allows for controlled variation of many physical properties such as electrical, thermal, and magnetic properties of the host. The enhancement of electrical conductivity has largely attracted the greatest attention. Improved electrical conductivity in intercalated graphite is due to a charge transfer from the intercalate layer where carriers have low mobility to graphite layers where the mobility is high. A large number of species can be intercalated into graphite and commonly classified as donor or acceptor compounds. Whether a chemical species intercalates depends on intercalant particle size and bonding distances as well as the associated chemical affinities and geometric constraints. Many of these compounds are unstable in air with donor compounds oxidizing easily and acceptor compounds being easily desorbed. Most intercalation compounds require encapsulation for chemical stability, but some that are stable in air include graphite-$FeCl_3$ and graphite-$SbCl_5$. Wang *et al.* introduced $FeCl_3$-GIC as a promising anode material for LIB. It delivered a discharge capacity of 665 mAh/g and a charge capacity of 506 mAh/g which is an initial coulombic efficiency of 76 %.[44] $FeCl_3$-GIC also showed good rate capability having a discharge capacity of 300 mAh/g at 5C which is 60 % capacity retention at a high charging rate. Furthermore, the presence of $FeCl_3$ inside the graphite host expands the interlayer distance allowing rapid diffusion of lithium ions. In another study, Li *et al.* introduced Fe_2O_3 molecules on the edge of $FeCl_3$-GIC compound to trap $FeCl_3$ and LiCl inside the graphite and prevent the outward diffusion of the chlorides. The material promised improved cycling stability with a reversible capacity as high as 1041 mAh/g at a current density of 200 mA/g and 91 % capacity

retention at high current density over 300 cycles.[24] Graphite intercalation compounds open possibilities for a high-capacity graphite material and provides a simple fabrication method for graphite/graphene-based materials.

Porous carbon-based composites (PCC) have also gained attention due to their unique properties that include large surface area, large pore volume, and unique pore size distribution. However, carbon materials with a broad range of pore sizes result in poor conductivity, low mass transportation, and low structural stability which hinders commercialization in catalytical and electrochemical applications. Therefore, efforts have been placed towards making high quality porous graphite material with adjustable pore size, narrow size distribution, large surface area and high conductivity from increased graphitization.[25] Furthermore, other active materials have been incorporated into porous carbon to enhance properties. For example, the carbon matrix allows facile electron transportation leading to high electronic conductivity and operation under high current. The active material in the matrix can lead to improved performance due to a synergistic environment. Porous structures facilitate electrolyte permeation which lead to greater electrode-electrolyte interface and this in turn provides more active sites for electrochemical and electrocatalytic reactions.[27] The small particle size of active materials also provides shorter diffusion paths for lithium ions during de-/intercalation process and result in higher rates of transport throughout the material.[26]

This work focuses on the development of porous graphite and on improving the rate performance as well as the initial coulombic efficiency of graphite. Pore structures in graphite would improve its kinetics by allowing faster lithium-ion diffusion and increase the amount of lithium-ion intercalation during the charging process, which in turn influences the cycling performance.

2 Materials and Methods

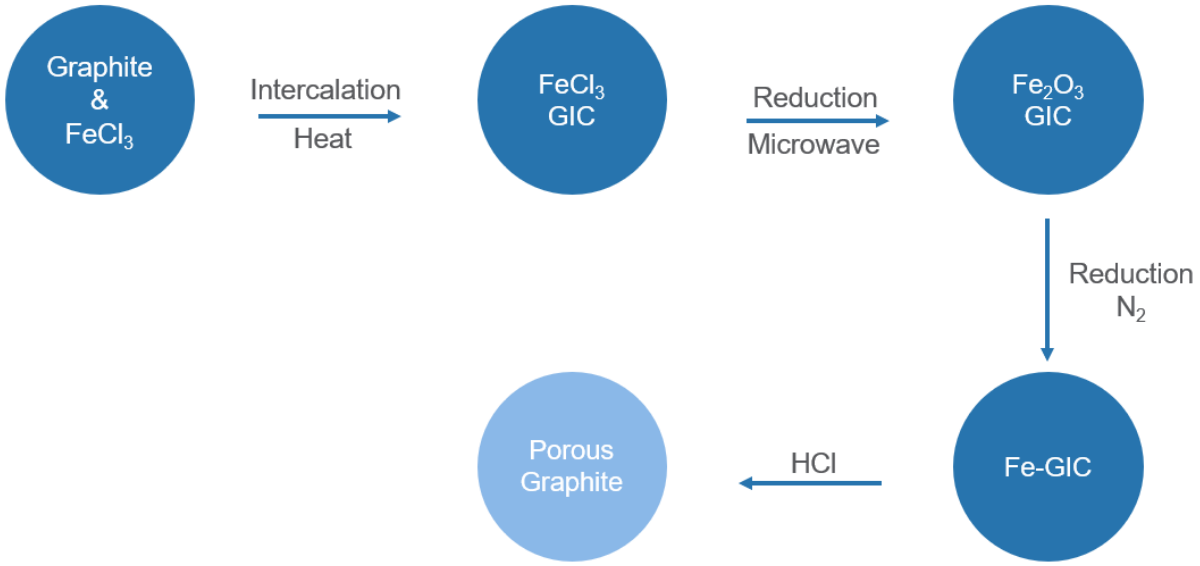

Figure 8. Procedure for the synthesis of porous graphite

2.1 Synthesis of $FeCl_3$-GIC

$FeCl_3$ (0.48 g, Alfa Aesar) and natural graphite (0.08 g, Sigma-Aldrich) was mixed thoroughly under Argon atmosphere. The mixture was transferred to an ampoule and vacuumed for 30 minutes. Then, the ampoule was sealed under vacuum and heated in air for 400°C for 24 hours with a heating rate of 5 °C/min. After cooling down, the powder was rinsed with ethanol to remove excess $FeCl_3$ and was dried at 60 °C. Finally, stage 1 $FeCl_3$-GIC was acquired.

2.2 Synthesis of Fe_2O_3-GIC

Stage 1 $FeCl_3$-GIC was transferred to a polypropylene container and underwent microwave irradiation at 700 watts in a microwave for 30 seconds. Fe_2O_3-GIC was obtained.

2.3 Synthesis of Fe-GIC

Fe_2O_3-GIC was reduced under Nitrogen atmosphere at 1000 °C for one hour with a step rate of 10 °C/min. After cooling down, Fe-GIC was obtained.

2.4 Synthesis of Porous Graphite

Fe-GIC was transferred to a solution of hydrochloric acid and distilled water (HCl/H_2O = 1:10). The mixture was stirred and heated at 100 °C for one hour. Then, it was ultrasonicated for ten minutes and filtered. The above steps were repeated twice. After drying the powder at 60 °C, porous graphite was obtained.

2.5 Materials Characterization

2.5.1. X-ray Diffraction (XRD)

Powder x-ray diffraction (XRD) was characterized by using the Rigaku Miniflex II diffractometer with Cu Kα radiation. The samples were scanned from 5 to 80 degrees at a rate of 5 degrees per minute.

2.5.2. Thermogravimetric Analysis (TGA)

TGA was performed with Netzsch STA449 F3 Jupiter. The samples were heated under Argon atmosphere up to 900 °C at a rate of 10 °C/min.

2.5.3. Scanning Electron Microscopy (SEM)

Morphology of the synthesized products was observed with SEM.

3 Results and Discussion

The synthesis method for $FeCl_3$-GIC is well developed. Li *et. al*, Zhang *et. al*, and Qi *et. al* used stainless-steel autoclaves in their syntheses while varying their mass ratios, heating time, and heating temperature.[24,37,48] After multiple attempts of replicating their procedures using the stainless-steel vessel, stage-1 $FeCl_3$-GIC could not be synthesized. A stainless-steel autoclave usually has a coating on the inside, and that coating could have worn out overtime with repeated use. The coating acted as a barrier and without that, it was possible that the $FeCl_3$ reacted with the stainless-steel walls which would result in side-reactions. Stainless-steel primarily contains iron, and when iron comes into contact with $FeCl_3$, $FeCl_2$ is formed.[15] A glass ampoule was used as the synthesis vessel instead for this reason.

The $FeCl_3$-GIC was transformed into Fe_2O_3-GIC by microwave irradiation. The irradiation generated heat rapidly to quickly transform the $FeCl_3$ while controlling the particle growth of the Fe_2O_3.[24] During the reduction reaction of Fe_2O_3-GIC, nitrogen gas was used to maintain an inert atmosphere while the graphite acted as the reducing agent. According to several studies, iron oxide can be potentially reduced by graphite when exposed to high temperatures and iron may be formed as well.[13,19] During this process, the heating rate was set to maximum of the furnace to avoid aggregation of iron oxide particles as much as possible. The particle size of iron oxides affects the reaction rate, and it was found that smaller particle size induces a higher reaction rate. In the final step, the iron atoms and remaining iron oxide particles (if any) was removed by rinsing with hydrochloric acid due to the acid's ability to dissolve iron.

3.1 Characterization: X-ray Diffraction

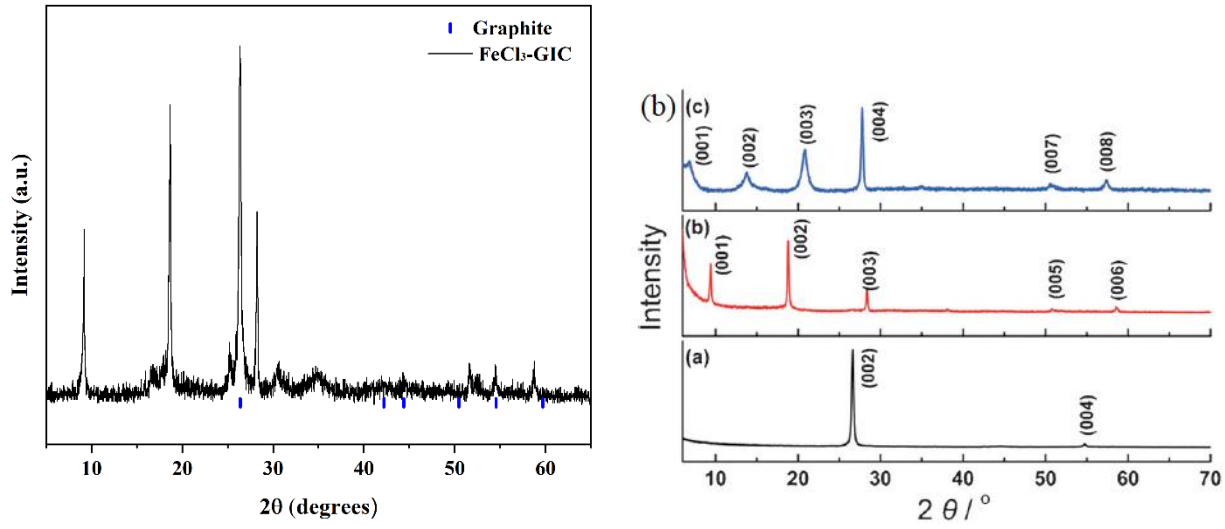

Figure 9. (a) XRD pattern of synthesized FeCl3-GIC. **(b)** Reference pattern of stage 1 $FeCl_3$-GIC (red) by Wang et.al.[45]

The XRD pattern for Stage-1 $FeCl_3$-GIC is shown in Figure 9a. The strong peaks at around 8°, 19°, 28°, 51°, and 57° are confirmed to be $FeCl_3$-GIC after comparison with several literature papers, one of which is referenced in Figure 9b (Wang, et al., 2013). However, one key difference is the intense graphite peak at 26° as marked by blue ticks in Figure 9a. This could be explained by considering the intercalation mechanism and diffusion rate of $FeCl_3$. Intercalation starts at the edge of the host graphite and the stage structure depends on the diffusion rate of $FeCl_3$ into the graphite. If diffusion of $FeCl_3$ is slow, the compound would only contain stage-1 at the edge and a large portion of unreacted graphite at the center of the flake. This is common in the reaction between the vapor of $FeCl_3$ and graphite.[46] Therefore, using this synthesis method can result in large amounts of unreacted graphite so it can be assumed that the graphite is not fully intercalated with $FeCl_3$.

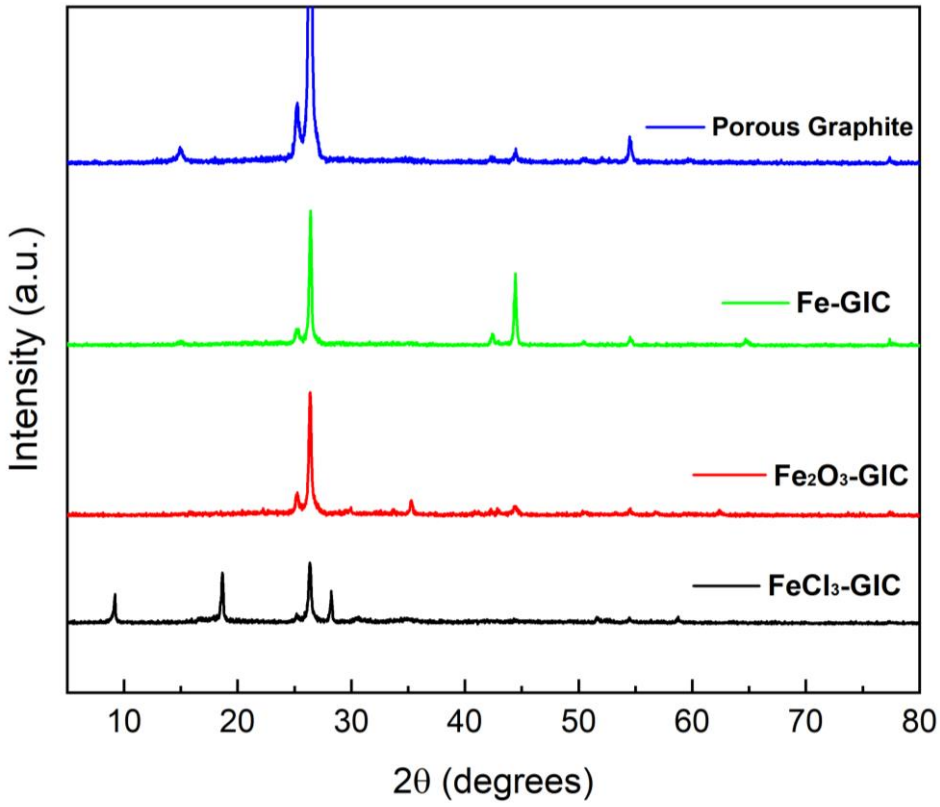

Figure 10. XRD pattern of $FeCl_3$-GIC (black), Fe_2O_3-GIC (red), Fe-GIC (green), and porous graphite (blue).

The peaks of stage-1 $FeCl_3$-GIC were absent after microwave as shown in Figure 10 although the peaks for Fe_2O_3 are difficult to decipher since the graphite peak is very strong. The weak peaks can also be due to the small amount of $FeCl_3$ intercalated as mentioned. Some Fe_2O_3 peaks are seen at 35.6°, 54°, 62.4°, and 77.7°. The XRD pattern of Fe-GIC is shown in Figure 10. The iron peaks are present at 44.7° and 65° which most likely indicates that all Fe_2O_3 was successfully reduced to Fe. Lastly, after rinsing Fe-GIC to remove all intercalants, all peaks belong to graphite with the exception to the peak at 15°.

3.2 Characterization: SEM

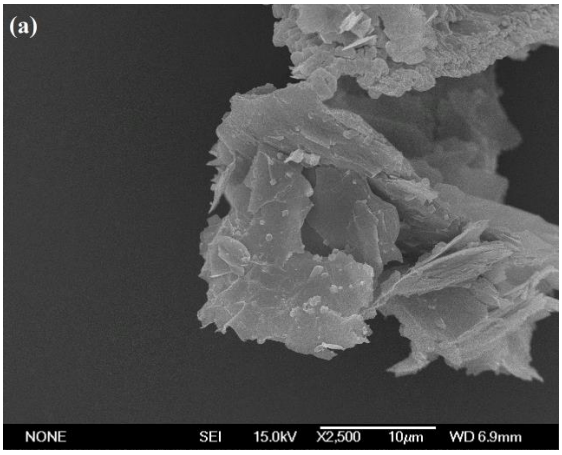

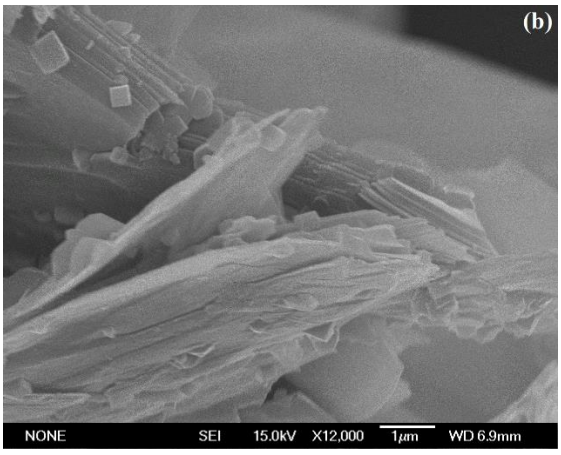

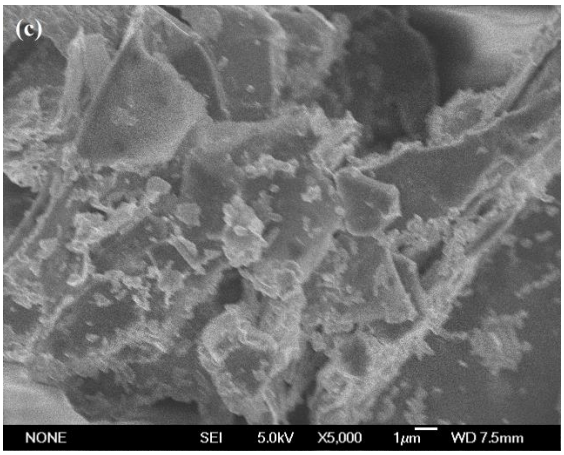

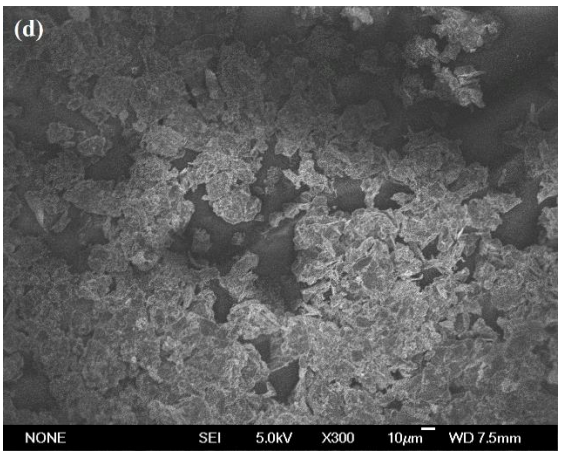

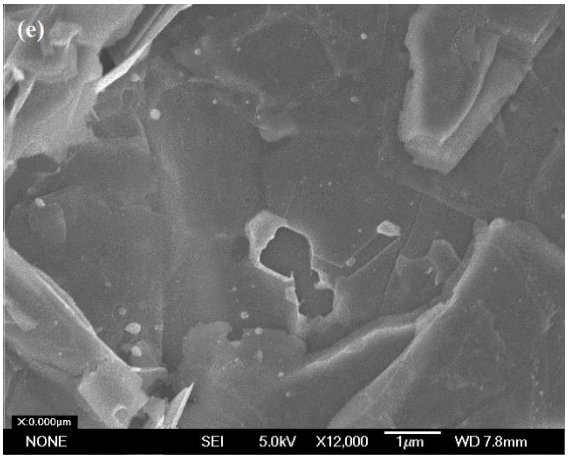

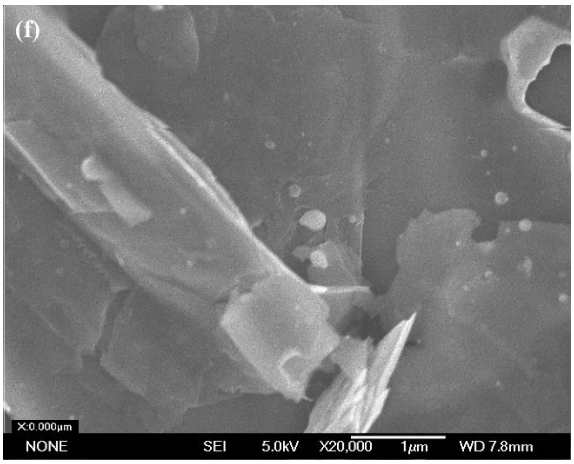

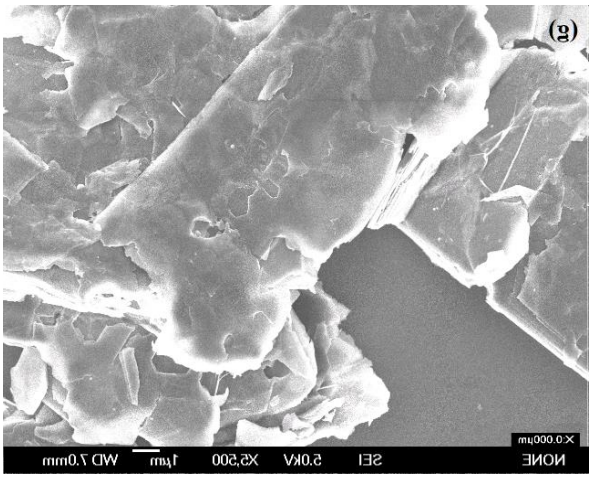

Figure 11. SEM of images of **(a-b)** Fe_2O_3-GIC after 20 s microwave. **(c-d)** Fe_2O_3-GIC after 30 s microwave. **(e-f)** Fe-GIC after reduction. **(g)** porous graphite after acid rinsing.

The morphology and microstructure of the prepared samples were studied using the SEM. Some lamellar structure of the graphite is maintained while most of it has been disoriented as observed after 20 s of microwave as shown in Figure 11a and Figure 11b. Fe_2O_3 particles are not well confined since there are many spherical particles found on the surface edge of the graphite and few remain inside the layers. Even more Fe_2O_3 particles are found on the surface after 30 s of microwave in Figure 11c and Figure 11d, which indicates that Fe_2O_3 amount depends on the irradiation time. However, it is uncertain whether the irradiation affects the interlayer distance of the graphite as it is difficult to distinguish based on the images. After the sample was reduced, it can be observed that there are some pore structures inside the graphite layers as in Figure 11e and Figure 11f. There seems to be many iron particles on the surface, with some within the pores and spanning several layers. Acid washing removed the iron particles leaving behind only pores on the graphite surface and inside the layers as shown in Figure 11g.

3.3 TGA

Table 1. Estimated amount of $FeCl_3$ and Fe_2O_3 by TGA.

Mass Ratio (graphite to $FeCl_3$)	Heating Time (Hr)	$FeCl_3$ Amount (%)	Fe_2O_3 Amount (%)
1:4	48	15.34	6.9
1:6	24	14.85	8.55

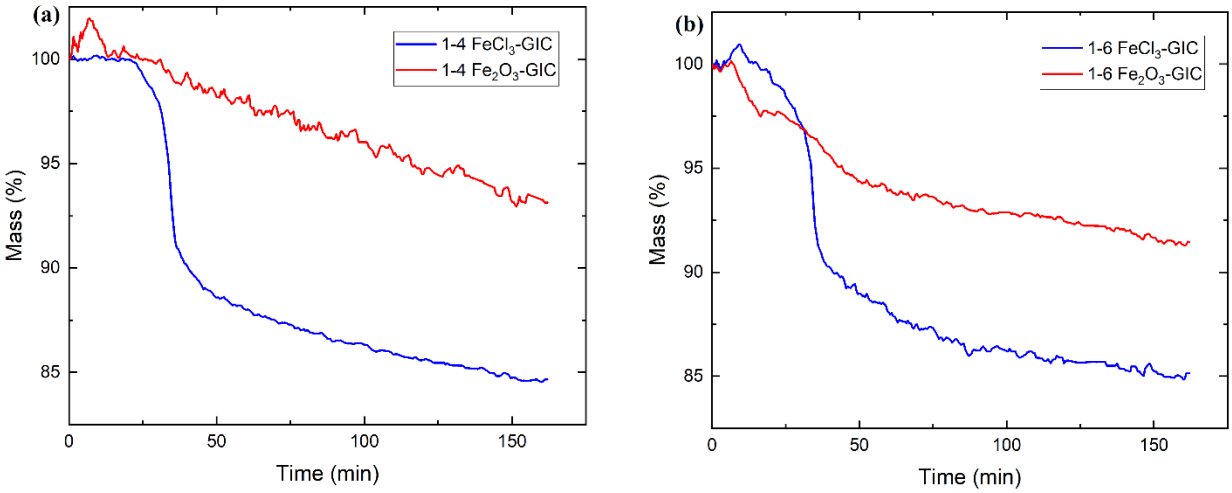

Figure 12. Comparison of TGA curves between **(a)** 1-4 FeCl3/Fe2O3-GIC and **(b)** 1-6 FeCl3/Fe2O3-GIC.

$FeCl_3$ was the facilitator in constructing the pores therefore it would be advantageous to intercalate as much $FeCl_3$ into the graphite layers as possible. Stage 1 $FeCl_3$-GIC allows for the greatest intercalants since stage-1 GICs are continuous stage structures. Mass ratios of 1:4 and 1:6 (graphite to $FeCl_3$) were experimented with to acquire a stage 1 $FeCl_3$-GIC with the greatest amount of $FeCl_3$. TGA was used to measure the mass composition of $FeCl_3$ and Fe_2O_3 in the stage-1 $FeCl_3$-GIC samples shown in Figure 12 and summarized in

Table *1*. Approximately 15 % of $FeCl_3$ was intercalated into graphite and about 7 % of Fe_2O_3 was attained using mass ratio of 1:4. Similarly, approximately 14.9 % of $FeCl_3$ was intercalated into graphite and 8.5 % of Fe_2O_3 was transformed with a mass ratio of 1:6. Intercalant content for both ratios vary minuscule therefore mass ratio of 1:6 was utilized for the synthesis because the sample could be retrieved in half the time frame. A synthesis using mass ratio 1:8

heated for 24 hours was attempted. Preliminary analysis of the 1:8 sample showed much weaker stage 1 peaks, so this was not pursued.

However, the $FeCl_3$ and Fe_2O_3 content in the graphite host was very small compared to a study carried by Li *et al.*, who were able to intercalate up to 63.8 % $FeCl_3$ by weight and transform 22.1 % to Fe_2O_3. This may also be attributed to the $FeCl_3$ not being inserted entirely into the layers.

3.4 Electrochemical Performance at High Current Rate

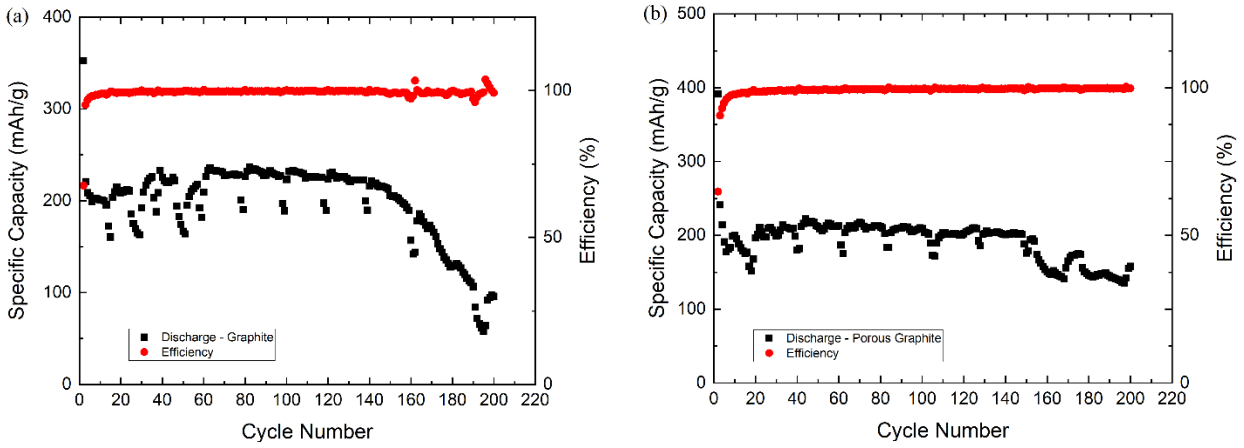

Figure 13. Specific capacity vs. cycle numbers of **(a)** graphite and **(b)** porous graphite at rate 1C.

The electrochemical performance of graphite and the porous graphite was assessed at various current rates, and the performance of both materials at current rate of 1 C is shown in Figure 13. As observed in Figure 13a, the first cycle discharge of graphite was 352.5 mAh/g and the second cycle discharge value dropped to 221.1 mAh/g, which was 62.7 % capacity retention. In Figure 13b where the first cycle discharge of porous graphite was 392 mAh/g and the second cycle discharge value dropped to 241.4 mAh/g, there was only 61.6 % capacity retention. Although the capacity of synthesized porous graphite increased by 11.2 % relative to pristine graphite, there was no outstanding improvement for the initial coulombic efficiency. This observation implies

negligible improvement in overall electrochemical performance. Secondly, the capacity of porous graphite and pristine graphite are fall in the same range during their life cycles, and it appeared to depreciate after 160 cycles. However, the pristine graphite exhibited a steeper and more rapid decline in performance after 160 cycles whereas the porous graphite depreciated steadily in activity overtime.

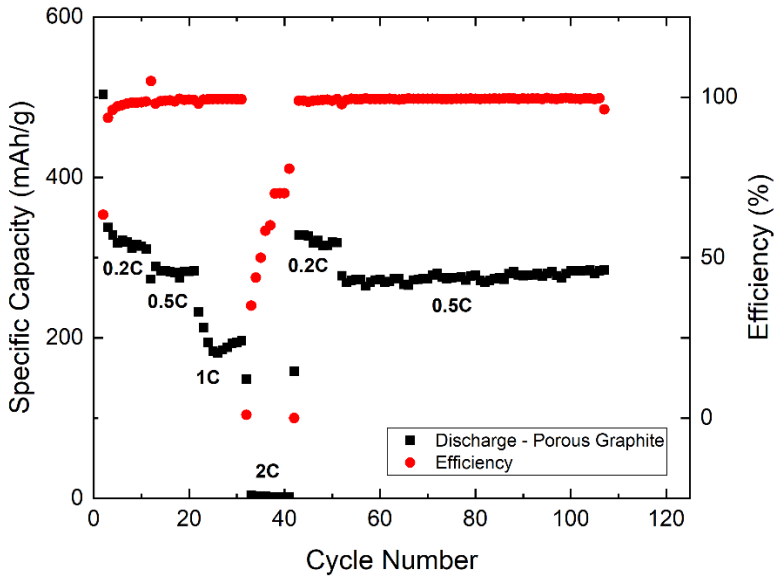

Figure 14. Rate performance of porous graphite.

The discharge curves of porous graphite at different discharge rates are shown in Figure 14. The cells were first charged from 0.2 C to 2 C, then remained at 0.5 C. There were no significant enhancements in cycling performance as it can be observed at a charging rate of 2 C, the capacity retention was nearly 0 %. The overall rate performance of porous graphite had no significant changes and it performed poorly at high current rate.

4 Conclusion

The objective of this project was to synthesize a graphite material that would have higher specific capacity and better rate performance and coulombic efficiency. A porous graphite structure would facilitate quicker de-/intercalation of lithium-ions into the graphene layers and permit more lithium-ions to be stored inside the host.

The observations made so far from XRD, SEM, and TGA suggested that the proposed synthesis method may have generated porous graphite as a product, but the final structure was not high quality. The XRD patterns showed strong graphite peaks for $FeCl_3$-GIC which suggested that $FeCl_3$ was not fully intercalated into the graphite host, and this affected the subsequent steps. Using the mass ratio of 1:6 (graphite to $FeCl_3$), 14.85 % $FeCl_3$ was intercalated into the graphite host, and only 8.55 % Fe_2O_3 was retained after transformation. Since a small amount of iron oxide was available in the layers, very few porous structures were managed to be created inside the graphite.

There was no significant improvement in the overall electrochemical performance. Although the specific capacity of the porous graphite appreciated by 11.2 % relative to the capacity value of the pristine graphite, the coulombic efficiency for each material was measured to be 61 – 63 %. The coulombic efficiency of the porous graphite would be higher ideally. Furthermore, the porous graphite demonstrated poor cycling performance. It exhibited poor capacity retention at 1 C and essentially 0 % capacity retention at 2 C.

The initial data collected suggests that the porous graphite developed in this project showed no significant improvement in electrochemical performance relative to pristine graphite. However, some modifications should be made to the synthesis procedure to better develop the porous graphite product before drawing final conclusions. The synthesis step for $FeCl_3$-GIC would be improved to intercalate more $FeCl_3$. Wang and Inagaki have shown that the diffusion rate of $FeCl_3$

increases in the presence of molten salts.[46] Furthermore, the final product would be characterized with BET to determine whether there is an increase in surface area relative to the pristine graphite.

In future work, another probable approach to consider is intercalating multiple chloride salts altogether or subsequently and then creating some porous structures while maintaining some of the intercalants inside the graphite host. This would attempt to attain higher anode capacity and improve the reaction kinetics of lithium-ion diffusion.

Beyond the scope of materials research, an area that still needs attention is recycling anode material such as graphite. Graphite has high demands for various technologies in LIB, fuel cells, and electronics which can lead to material shortage in the long term. Furthermore, anode materials that are not properly disposed can cause pollution and pose hazardous conditions for the environment and human health.[51] Developing methods to purify and recycle spent graphite would alleviate the shortage of graphite resources and contribute to the future of sustainable energy.

5 References

1. Al, X., Weaving, J. S., Coowar, F., Teagle, D. A., Cullen, J., Dass, V., . . . Macklin, W. J. (2001). Development of high energy density Li-ion batteries based on LiNi1AxAy Co. *Journal of Power Sources, 97-98*, 733 - 735. doi:10.1016/S0378-7753(01)00700-5
2. Allart, D., Montaru, M., & Gualous, H. (2018). Model of Lithium Intercalation into Graphite by Potentiometric Analysis with Equilibrium and Entropy Change Curves of Graphite Electrode. *Journal of The Electrochemical Society, 165*(2), A380 - A387. doi:10.1149/2.1251802JES
3. Armand, M. B. (1980). Intercalation Electrodes. (N. C. Science), Ed.) *Materials for Advanced Batteries, 2*, 145 - 161. doi:10.1007/978-1-4684-3851-2_7
4. Asenbauer, J., Eisenmann, T., Kuenzel, M., Kazzazi, A., Chen, Z., & Bresser, D. (2020). The success story of graphite as a lithium-ion anode material – fundamentals, remaining challenges, and recent developments including silicon (oxide) composites. *Sustainable Energy & Fuels, 4*(11), 5387-5416. doi:10.1039/d0se00175a
5. Azuma, H., Imoto, H., Yamada, S., & Sekai, K. (1999). Advanced Carbon Anode Materials for Lithium Ion Cells. *Journal of Power Sources, 81 - 82*, 1 - 7. doi:10.1016/S0378-7753(99)00122-6
6. Burns, J. C., Sinha, N. N., Coyle, D. J., Jain, G., VanElzen, C. M., Lamanna, W. M., . . . Dahn, J. R. (2012). The Impact of Varying the Concentration of Vinylene Carbonate Electrolyte Additive in Wound Li-Ion Cells. *J. Electrochem. Soc., 159*(2), A85 - A90.
7. Cho, J., & Thackeray, M. M. (1999). Structural Changes of LiMn 2 O 4 Spinel Electrodes during Electrochemical Cycling. *Journal of The Electrochemical Society, 146*(10), 3577-3581.

8. Daumas, N., & Herold, A. (1969). *C. R. Hebd. Seances Acad. Sci., 268*, 373.
9. Ding, F., Xu, W., Choi, D., Wang, W., Li, X., Engelhard, M. H., . . . Zhang, J.-G. (2012). Enhanced performance of graphite anode materials by AlF 3 coating for lithium-ion batteries. *J. Mater. Chem*, 12745 - 12751. doi:10.1039/c2jm31015e
10. Ein-Eli, Y., & Koch, V. (1997). Chemical Oxidation: A Route to Enhanced Capacity in Li-Ion Graphite Anodes. *J. Electrochem. Soc.*, 2968 - 2973.
11. Feng, T., Xu, Y., Zhang , Z., Du, X., Sun, X., Xion, L., . . . Holze, R. (2016). Low-Cost Al 2 O 3 Coating Layer As a Preformed SEI on Natural Graphite Powder To Improve Coulombic Efficiency and High-Rate Cycling Stability of Lithium-Ion Batteries. *Applied Materials and Interface*, 612 - 6519. doi:10.1021/acsami.6b00231
12. Fleischhammer, M., Waldmann, T., Bisle, G., Hogg, B.-I., & Wohlfahrt-Mehrens, M. (2015). Interaction of cyclic ageing at high-rate and low temperatures and safety in lithium-ion batteries. *Journal of Power Sources*, 432 - 439.
13. Hisa, M., Tsutsumi, A., & Akiyama, T. (2004). Reduction of Iron Oxides by Nano-Sized Graphite Particles Observed in Pre-Oxidized Iron Carbide at Temperatures around 873K. *Materials Transactions, 45*(6), 1907 - 1910.
14. Hofmann, U., & Rudorff, W. (1938). *Transaction of the Faraday Society, 45*, 1017 - 1021.
15. Hooley, J. G., Bartlett, M. W., Liengme, B. V., & Sams, J. R. (1968). A Mossbauer Study of Graphite Iron Chloride Compounds. *Carbon*, 681 - 685.
16. Hu, Y., Kong, W. H., Li, H., Huang, X., & Chen, L. (2004). Experimental and Theoretical Studies on Reduction Mechanism of Vinyl Ethylene Carbonate on Graphite Anode for Lithium Ion Batteries. *Electrochem. Commun., 6*(2), 126 - 131.

17. Idota, Y., Kubota, T., Matsufuji, A., & Maekawa, Y. (1997). Tin-Based Amorphous Oxide: A High-Capacity Lithium-Ion-Storage Material. *Science, 276*, 1395−1397.

18. Jung, Y. S., Cavanagh, A. S., Riley, L. A., Kang, S.-H., Dillon, A. C., Groner, M. D., . . . Lee, S.-H. (2010). Ultrathin Direct Atomic Layer Deposition on Composite Electrodes for Highly Durable and Safe Li-Ion Batteries A ð. *Advanced Materials*, 2172 - 2176.

19. Kasai, E., Mae, K., & Saito, F. (1995). Effect of Rnixed-grinding Material and lron Oxide. *ISIJ International, 35*(12), 1444 - 1451.

20. Kasavajjula, U., Wang, C., & Appleby, A. J. (2007). Nano-and Bulk-Silicon- Based Insertion Anodes for Lithium-Ion Secondary Cells. *J. Power Sources, 163*, 1003 - 1039.

21. Kresse, G. (1996). Efficiency of ab-Initio total energy calculations for metals and semiconductors using a plane-wave basis set. *J. Comput. Mater. Sci*, 15 - 50.

22. Kuhne, M., Paolucci, F., Ostrovsky, P., Maier, J., & Smet, J. (2017). Ultrafast lithium diffusion in bilayer graphene. *Nature Nanotechnology*, 895 - 900. doi:10.1038/NNANO.2017.108

23. Kurzweil, P. (2015). Lithium Battery Energy Storage: State of the Art Including Lithium–Air and Lithium–Sulfur Systems. *Electrochemical Energy Storage for Renewable Sources and Grid Balancing*, 269 - 307. doi:10.1016/B978-0-444-62616-5.00016-4

24. Li, Z., Zhang, C., Han, F., Zhang, F., Zhou, D., Xu, S., . . . Liu, J. (2019, 06 04). Improving the cycle stability of FeCl3-graphite intercalation compounds by polar Fe2O3 trapping in lithium-ion batteries. *Nano Research, 12*(8), 1836 - 1844. doi:10.1007/s12274-019-2444-2

25. Liang, C., Li, Z., & Dai, S. (2008). Mesoporous Carbon Materials: Synthesis and Modification. *Angewandte Chemie, 47*(20), 3696-3717. doi:10.1002/anie.200702046

26. Liu, H., & Wang, G. (2014). An investigation of the morphology effect in Fe2O3anodes for lithium ion batteries. *J. Mater. Chem. A*, 9955. doi:10.1039/c4ta01544d

27. Liu, H., Liu, X., Li, W., Guo, X., Wang, Y., Wang, G., & Zhao, D. (2017). Porous Carbon Composites for Next Generation Rechargeable Lithium Batteries. *Advanced Energy Materials, 7*(24), 1700283. doi:10.1002/aenm.201700283

28. Lu, J., Chen, Z., Pan, F., Cui, Y., & Amine, K. (2018). High-Performance Anode Materials for Rechargeable Lithium-Ion Batteries. *Electrochemical Energy Reviews*, 35 - 53. doi:10.1007/s41918-018-0001-4

29. Luders, C. v., Zinth, V., Erhard, S. V., Osswald, P. J., Hofmann, M., Gilles, R., & Jossen, A. (2017). Lithium plating in lithium-ion batteries investigated by voltagerelaxation and in situ neutron diffraction. *Journal of Power Sources*, 17 - 23. doi: 10.1016/j.jpowsour.2016.12.032

30. Mogi, R., Inaba, M., Jeong, S.-K., Iriyama, Y., Abe, T., & Ogumi, Z. (2002). Effects of some organic additives on lithium deposition in propylene carbonate. *J. Electrochem. Soc., 149*(12), A1578 - A1583.

31. Nishi, Y. (2001). Lithium ion secondary batteries; past 10 years and the future. *Journal of Power Sources, 100*(1-2), 101 - 106. doi:10.1016/s0378-7753(01)00887-4

32. Nobili, F., Dsoke, S., Mancini, M., Tossici, R., & Marassi, R. (2008). Electrochemical investigation of polarization phenomena and intercalation kinetics of oxidized graphite electrodes coated with evaporated metal layers. *Journal of Power Sources, 180*(2), 845 - 851. doi:10.1016/j.jpowsour.2008.02.069

33. Nobili, F., Dsoke, S., Mecozzi, T., & Marassi, R. (2005). Metal-oxidized graphite composite electrodes for lithium-ion batteries. *Electrochimica Acta, 51*(3), 536 - 544. doi:10.1016/j.electacta.2005.05.012

34. Peled, E., Menachem, C., Bar-Tow, D., & Melman, A. (1996). Improved graphite anode for Lithium-Ion Batteries Chemically: Bonded solid electrolyte interface and Nanochannel formation. *Journal of The Electrochemical Society, 143*, L4 - L7. doi:10.1149/1.1836372

35. Persson, K., Sethuraman, V. A., Hardwick, L. J., Hinuma, Y., Meng, Y. S., van der Van, A., . . . Ceder, G. (2010). Lithium Diffusion in Graphitic Carbon. *J. Phys. Chem. Lett, 1*, 1176 - 1180. doi:10.1021/jz100188d

36. Petzl, M., & Danzer, M. A. (2014). Nondestructive detection, characterization, and quantificationof lithium plating in commercial lithium-ion batteries. *Journal of Power Sources*, 80 - 87.

37. Qi, X., Qu, J., Zhang, H.-B., Yang, D., Yu, Y., Chi, C., & Yu, Z.-Z. (2015). FeCl3intercalated few-layer graphene for high lithium-ion storage performance. *Journal of Materials Chemistry A, 3*(30), 15498 - 15504. doi:10.1039/c5ta03087k

38. Sahore, R., Dogan, F., & Bloom, I. D. (2019). Identification of Electrolyte-Soluble Organic Cross-Talk Species in a Lithium-Ion Battery via a Two-Compartment Cell. *Chem. Mater., 31*(8), 2884 - 2891. doi:10.1021/acs.chemmater.9b00063

39. Serp, P. (2013). Carbon. *Comprehensive Inorganic Chemistry II*, 323 - 369. doi:10.1016/b978-0-08-097774-4.00731-2

40. Sharova, V., Moretti, A., Giffin, G., Carvalho, D., & Passerini, C. (2017). Evaluation of Carbon-Coated Graphite as a NegativeElectrode Material for Li-Ion Batteries. *C, Journal of Carbon Research, 3*(22), 1 - 11. doi:10.3390/c3030022

41. Song, X. Y., Kinoshita, K., & Tran, T. D. (1996). Microstructural Characterization of Lithiated Graphite. *Journal of The Electrochemical Society, 143*(6), L120 - L123. doi:10.1149/1.1836896

42. Waldmann, T., & Wohlfahrt-Mehrens, M. (2017). Effects of rest time after Li plating on safety behavior—ARC tests with commercial high-energy 18650 Li-ion cells. *Electrochimica Acta*, 454 - 460.

43. Waldmann, T., Wilka, M., Kasper, M., Fleischhammer, M., & Wohlfahrt-Mehrens, M. (2014). Temperature dependent ageing mechanisms in Lithium-ionbatterieseA Post-Mortem study. *Journal of Power Sources*, 129 - 135.

44. Wang, F., Yi, J., Wang, Y., Wang, C., Wang, J., & Xia, Y. (2014). Graphite Intercalation Compounds (GICs): A New Type of Promising Anode Material for Lithium-Ion Batteries. *Materials Views*, 1 - 6. doi:10.1002/aenm.201300600

45. Wang, L., Zhu, Y., Guo, C., Zhu, X., Liang, J., & Qian, Y. (2013). Ferric chloride-Graphite Intercalation Compounds as Anode Materials for Li-ion Batteries. *ChemSusChem, 7*(1), 87-91. doi:10.1002/cssc.201300874

46. Wang, Z., & Inagaki, M. (1991). Intercalation of FeCl3 into graphite films in molten salts. *Synthetic Metals, 44*(2), 165 - 176. doi:10.1016/0379-6779(91)91832-u

47. Zhan, C., Wu, T., Lu, J., & Amine, K. (2018). Dissolution, migration, and deposition of transition metal ions in Li-ion batteries exemplified by Mn-based cathodes-a critical review. *Energy Environ. Sci, 11*, 243 - 257. doi:10.1039/c7ee03122j

48. Zhang, C., Ma, J., Han, F., Liu, H., Zhang, F., Fan, C., . . . Li, X. (2018). Strong anchoring effect of ferric chloride-graphite intercalation compounds (FeCl3-GICs) with tailored epoxy groups for high-capacity and stable lithium storage. *Journal of Materials, 6*(37), 17982 - 17993. doi:10.1039/c8ta06670a

49. Zhang, H., Yang, Y., Dongsheng, R., Wang, L., & He, X. (2020). Graphite as anode materials: Fundamental mechanism, recent progress and advances. *Energy Storage Materials, 36*, 147 - 170. doi:10.1016/j.ensm.2020.12.027

50. Zhang, S. S. (2006). A review on electrolyte additives for lithium-ion batteries. *J. Power Sources, 162*(2), 1379 - 1394. doi:10.1016/j.jpowsour.2006.07.074

51. Gao, Y., Wang, C., Zhang, J., Jing, Q., Ma, B., Chen, Y., & Zhang, W. (2020). Graphite recycling from the spent lithium-ion batteries by sulfuric acid curing–leaching combined with high-temperature calcination. *ACS Sustainable Chemistry & Engineering*, *8*(25), 9447–9455. https://doi.org/10.1021/acssuschemeng.0c02321